Diamond & Related Materials 93 (2019) 1–7

Contents lists available at ScienceDirect

Diamond & Related Materials

journal homepage: www.elsevier.com/locate/diamond

Electrical conductivity of double textured black diamond films from RT to 800 K

A. Orsini[a,*], A. Bellucci[b], M. Girolami[b], M. Mastellone[b], S. Orlando[c], G. Prestopino[d], V. Valentini[b], S. Salvatori[a], D.M. Trucchi[b]

[a] Università degli Studi Niccolò Cusano, Via Don Carlo Gnocchi, 3, Rome, Italy
[b] Istituto di Struttura della Materia, ISM-CNR, via Salaria km. 29.300, Rome, Monterotondo, Italy
[c] Istituto di Struttura della Materia, ISM-CNR, Tito Scalo, Potenza, Italy
[d] Università di Roma "Tor Vergata", Via del Politecnico, 1, Rome, Italy

ARTICLE INFO

Keywords:
Diamond films
LIPSS
Electric conductivity
Activation energy
Thermal annealing

ABSTRACT

Black diamond films represent examples of defect-engineered materials with enhanced optical and photoelectronic properties for applications at high temperatures and in harsh environments. Up to now, no scientific study about the electronic transport properties in the dark on the treated side has been reported as a function of temperature. Experimental results highlight that double-textured black diamond samples, obtained by two successive laser treatments along each orthogonal direction of diamond substrates, have electric transport characterized by two activation energies. The first one is responsible for the room-temperature conduction, with values comparable to the thermal energy at 300 K (tens of meV) and the second one appearing around 550 K, with values ranging from 0.45 of eV to almost 1.74 eV in the different samples. Interestingly, as the fraction of accumulated fluence released during the first of the two treatments decreases, the activation energy at high temperature of the samples increases, as well as the instability of electric conductivity after thermal annealing, that in turn induces a decrease of all the activation energies down to about 0.3–0.4 eV.

1. Introduction

The possibility to transform optical grade transparent diamond substrates into substrates with very high visible-light absorption coefficient by means of femtosecond Laser Induced Periodic Surface Structuring (LIPSS) generated the characterizing terminology of "black diamond" (BD) [1]. Such material combines the aforesaid high absorptance with a low electron affinity if hydrogen-terminated, key property to increase performances in Photo-Enhanced Thermionic Emitters (PETE) [2,3]. The possible implementation of such substrates into PETE devices at the temperatures related to such technological application makes the characterization in temperature of the electronic properties of black diamond samples very important. The change of light absorption with different doses of laser energy indicates that the energy levels introduced inside the 5.47 eV diamond bandgap can somehow be tuned [4,5]. The common way to create controlled defects in diamond energy gap is the boron substitutional doping, with activation energy ranging from 0.36 eV down to 0.27 eV, depending on the quality level of the polycrystalline thin film [6]. Clearly, the defects created by substitutional doping and their relative activation energies are different from the defects created by the laser energy release over the diamond surface. On the other hand, research studies over thermal behavior of electrical conduction in boron-doped diamond films are valid comparison terms especially for hopping transport phenomena between charged and neutral dopant atoms, prevalent in the low temperature range with activation energies around 25 meV [7]. A large increase of boron doping up to 10^{20}–10^{21} cm^{-3} can even make electron hopping the room temperature prevalent mechanism of charge transport [8]. A third activation energy, corresponding to hole transport over neutral impurity, may also appear into electrical characterization of homoepitaxial boron doped diamond films but such conduction mechanism only rarely prevail in the temperature range between valence band and hopping transport [9,10].

A common element like Nitrogen is the most efficient substitutional element for carbon in the n-type doping of diamond, but it corresponds to a deep level of 1.7 eV [11] and therefore to high levels of resistivity. A different behavior is expected when nanograins with size of < 5 nm form diamond (UNCD), because of the easiness of Nitrogen to be incorporated into the grain-boundaries [12]. Best conductivity for UNCD equals to 150–200 S/cm [12,13], with Ikeda et al. clarifying that such

* Corresponding author at: Università degli Studi Niccolò Cusano, Via Don Carlo Gnocchi, 3, Rome 00166, Italy.
E-mail address: andrea.orsini@unicusano.it (A. Orsini).

https://doi.org/10.1016/j.diamond.2019.01.011
Received 20 September 2018; Received in revised form 15 January 2019; Accepted 15 January 2019
Available online 16 January 2019
0925-9635/

behavior is mainly due to sp^2 clustering at the grain boundaries more than nitrogen doping of the diamond. In fact, the increase of sp^2 phase order, before to negatively affect carriers mobility, increases the electron concentration and lowers the resistivity [14].

In this paper, we characterize double-textured 2T-BD films in which lattice defects are intentionally created into polycrystalline diamond substrates by fast restructuring of the carbon bonds after laser high-energy pulses irradiation, distributed along two perpendicular geometrical directions corresponding to the substrate sides in order to create a pseudo 2T surface periodicity. These defects may act as traps for charge carriers, as well as recombination centers. In a recent paper, we showed that, through a proper choice of the accumulated laser fluence split ratio between the two steps of the texturing process, analyzed also in terms of residual structural stress, it is possible to obtain unprecedented solar absorptance values for a black diamond film (exceeding 99%), thus launching double-nanotextured black diamond as a possible alternative to black silicon as absorbing layer for high-efficiency solar cells and solar thermal receivers [15].

2. Experimental

The original substrates are thermal-grade polycrystalline CVD diamond samples purchased from Element Six Ltd. with square shape. Lateral size is 10 mm and thickness is 250 ± 25 μm. Such substrates were mounted in a high-vacuum chamber and LIPSS were induced over their surface by using a linearly polarized femtosecond pulsed laser beam (further details are given elsewhere [15]). We divided the total chosen laser delivered energy in different percentages between treatments along two perpendicular axes parallel to the diamond sides (2T-BD). The total accumulated laser fluence used at a laser wavelength of 800 nm for 1 square centimeter diamond surface was 5.0 kJ, that demonstrated to be the optimized value for light absorptance in previous studies [4]. In this work we analyzed four samples of type 2T-BD: 2T-9010, 2T-8020, 2T-6633 and 2T-5050, where the first two digits represent the fraction of accumulated fluence released during the first treatment and the last ones the related complement to 100%, released during the second treatment (e.g. 2T-9010 has the 90% of the total accumulated fluence given in the first axis and 10% given in the perpendicular one and so on).

In the case of 2T-9010, ripples with a spatial frequency of about 170 nm are created perpendicularly to the laser beam direction of polarization. This sample resembles the structures of 1T-sample created at the same laser wavelength (800 nm). On the other hand, in 2T-8020 there is still the same geometrical imprinting over the diamond surface but there is a slight broadening and a loss of continuity in the ripples, interrupted by 45° oblique grooves. The ripples alignment is completely lost in 2T-6633 sample, where ripples are very short, with very small height and 45°-135° slantingly inclined. Well formed, long and ordered ripples are recovered in 2T-5050 sample but with a direction perpendicular to the 2T-9010 case, as expected by the 90° rotation of the laser beam polarization in the second treatment. The sample with an accumulated fluence fraction of 66% released during the first step revealed as the most sunlight-absorbing among them. In general, it was demonstrated that the samples with a lower fraction of accumulated fluence during the first step actually absorbed a higher value of laser fluence [15]. This is due to the incubation effect that induces an incremental absorption of the laser beam along with the number of pulses under the same conditions.

In order to perform electrical transport measurements, two rectangular silver electrodes with dimensions of 8 mm × 3 mm with intergap of 1.0 mm were sputtered over the laser treated surface of all the previously mentioned samples. In such a way it is possible to relate the measured resistance R to the resistivity ρ in a standard and repeatable way for all the samples. Unfortunately, although the LIPSS depth is known to be about 500 nm, the thickness of the conductive layer is unknown, since the conductive layer could be even corresponding to few atomic planes under the surface. Therefore, it is not possible to derive the actual resistivity value but it is only possible to realize a comparative study between the investigated samples. Electronic properties of each sample were tested in high-vacuum chamber with pressure lower than 10^{-7} mbar. Temperature was adjusted by controlling the current flowing through a tantalum wire embedded into a boron nitride and copper holder where the diamond substrate was mechanically fixed by pressing metallic molybdenum tips. The tantalum wire was supplied by a staircase stepped voltage in order to have different copper base temperatures, which value and time stabilization was measured with a platinum thermistor adhered to it by silver paste. At each steady-state thermal point a dark current to voltage $I(V)$ characteristic was measured with positive and negative symmetrical supply voltages ranging from 0 V to 40 V and from 0 V to −40 V by using a Keithley 2440 sourcemeter.

Samples were also investigated by means of Raman spectroscopy analysis, acquired in the 1110–1677 cm^{-1} range at room temperature with an Ar^+ laser (514.5 nm wavelength), in back-scattering geometry, by using a Dilor XY triple spectrometer equipped with a liquid nitrogen-cooled charge coupled device detector and an adapted Olympus microscope arranged in confocal mode; the spot size was 2 μm.

3. Results and discussion

3.1. Electrical transport

We collected and analyzed all the temperature dependent $I(V)$ curves to calculate the resistance in the following way: we extracted with a simple linear fit two resistance values, one for positive and one for negative applied voltages. In Fig. 1 the linear behavior of such curves for the sample 2T-8020 is shown at different temperature T. A little non-linear region was observed only in sample 2T-9010 around the axes origin probably due to non-ideal ohmic nature of contacts, therefore for this sample we excluded the current values at low voltage ($-10\,V < V < 10\,V$) from the linear fit for the resistance calculation.

We reported in Fig. 2 the thermal behavior of the resistance of the four different black diamond samples arranged into an Arrhenius plot. Measurements clearly show the presence of two activation regimes, with a slope change of the resistance at about 550 K (about 280 °C).

The used model to fit the data is a very simple approximation with two thermally activated populations of conducting charges inducing the conductance G with E_{a1} and E_{a2} activation energies as a function of the absolute temperature T:

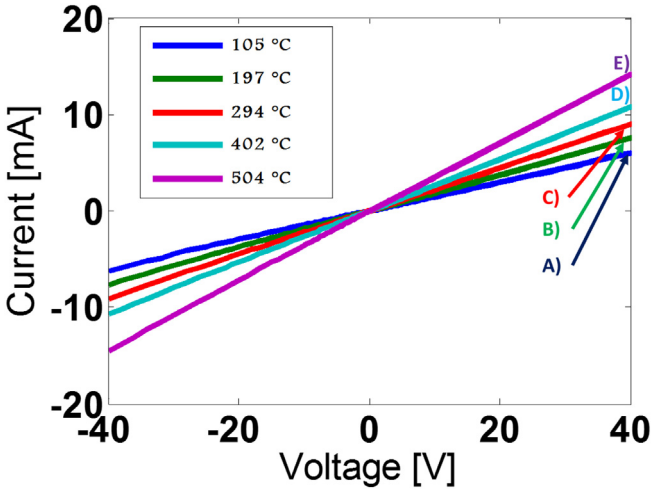

Fig. 1. I/V curves of sample 2T-8020 at different temperatures: A) 105 °C blue curve; B) 197 °C green curve; C) 294 °C red curve; D) 402 °C azure curve and E) 504 °C purple curve. (For interpretation of the references to color in this figure legend, the reader is referred to the web version of this article.)

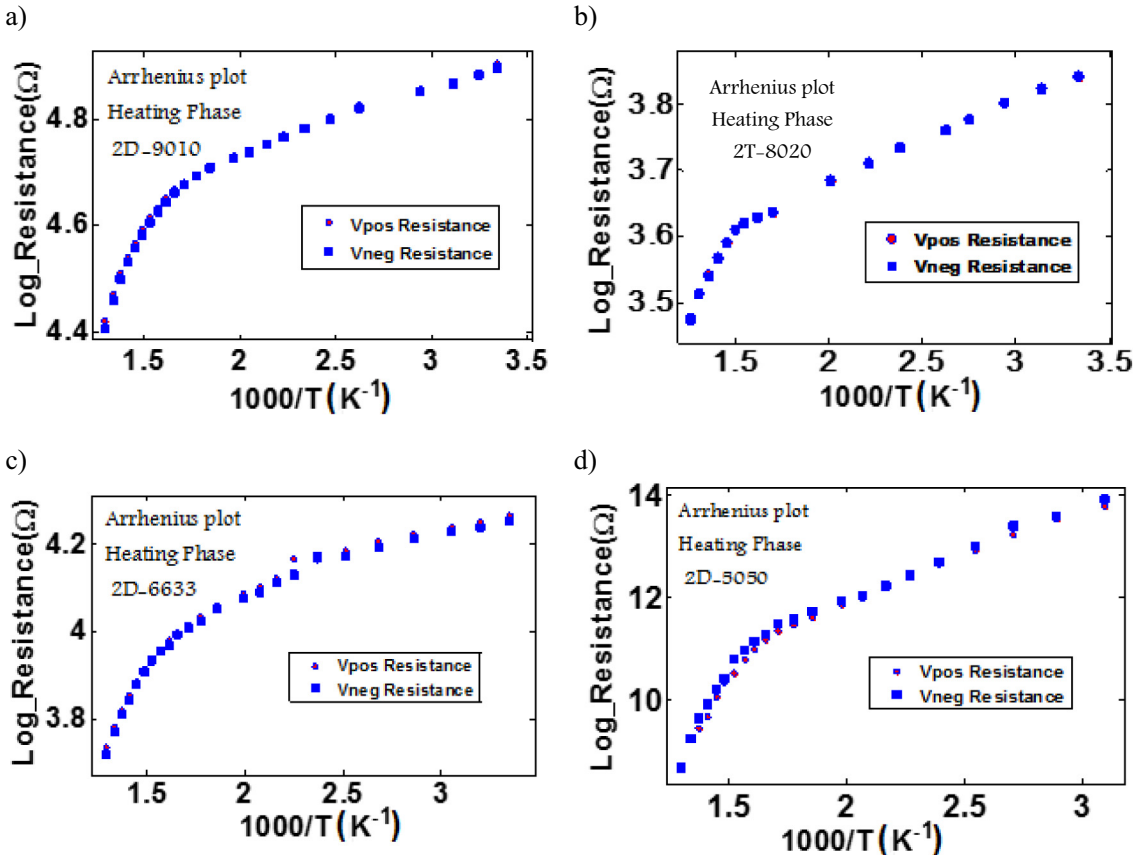

Fig. 2. Arrhenius plots of the four type of samples: a) 2T-9010 b) 2T-8020 c) 2T-6633 e d) 2T-5050. Red Circles represent the resistance in the 1 quadrant of the I/V curve and the blue squares the resistance in the third quadrant of the I/V curve. (For interpretation of the references to color in this figure legend, the reader is referred to the web version of this article.)

$$G = G_{PreF1}\cdot e^{-\frac{E_{a1}}{k_B\cdot T}} + G_{PreF2}\cdot e^{-\frac{E_{a2}}{k_B\cdot T}} = G_{PreF1}\cdot e^{-\frac{E_{a1}}{k_B\cdot T}}\cdot\left(1 + r_G\cdot e^{-\frac{E_{a2}-E_{a1}}{k_B\cdot T}}\right)$$

$$\log(R) = -\log(G_{PreF1}) + \frac{\log(e)\cdot E_{a1}}{k_B\cdot T} - \log\left(1 + r_G\cdot e - \frac{E_{a2}-E_{a1}}{k_B\cdot T}\right)$$

where k_B is the Boltzmann constant, G_{PreF1} and G_{PreF2} the low- and high-temperature conductance Pre-exponential factors, respectively. The parameter $r_G = G_{PreF2}/G_{PreF1}$ in the latter equation has been introduced to simplify the fitting procedure used to estimate the mentioned parameters. We can consider a first region up to temperatures < 280 °C (corresponding to $1000/T$ values > 1.8 K^{-1}) where the experimental points of the Arrhenius plot are fitted by applying the one activation energy model thus deriving the low-temperature activation energy E_{a1} and conductance G_{PreF1}. The activation energy E_{a1} is in the order of 20 meV with exception of the sample 2T-5050, reporting a value of 0.37 eV (see Table 1). Afterwards, by using the previous calculated values for E_{a1} and $\log(G_{PreF1})$ we apply a best fit procedure to the overall temperature range to obtain the other two missing parameters E_{a2} and r_G. Table 1 summarizes the activation energies extracted from Arrhenius plots shown in Fig. 2. In particular, we fitted all the plots by using the model with two activation energies reported before, except for the c) plot corresponding to the 2T-6633 sample, that was fitted with a three activation energies model (causing two activation energies at low temperature).

Table 1
Fitted parameters of the BD samples as measured during the heating phase.

Sample	*Low temperature range*		*High temperature range*	
	E_{a1} *(eV)*	G_{PreF1} *(S)*	E_{a2} *(eV)*	G_{PreF2} *(S)*
2T-9010	15 m	0.033 m	0.45	0.017
2T-8020	25 m	0.37 m	0.69	1.8
2T-6633	18 m, 0.24	0.11 m	0.75	3.2
2T-5050	0.37	6.7 n	1.74	370

Although a clear trend is not observable in the low temperature range, for T > 550 K it is worth to note an increase in both the conductance Pre-Factor and the activation energy values according to a higher laser energy absorbed by the samples (or, equally, corresponding to a lower fraction of accumulated fluence during the first treatment). We remark that in the second orthogonal surface texturing, the diamond surface acts already as absorbing “black diamond” and gets an even major amount of laser energy, therefore the defects creation in the films increases with the percentage division that indicates the sample name. [15] Therefore, we directly relate the appearance of a low activation energy in the low temperature range as a possible charge hopping phenomena from defect to defect with a maximum concentration (Prefactors value) in the 2T-8020 and 2T-6633 samples, the ones showing a slantingly continuous modification of the LIPSS. Conversely, in the high temperature range the high value of E_{a2} = 1.74 eV in 2T-5050 let us suggest Nitrogen impurity acting as donors as the prevalent mechanism of conduction [16]. This value gradually slows in the samples with less grade of double texturing.

Furthermore, in Fig. 3 we superimpose the $I(V)$ curve at RT before rising temperature to 800 K (red curve) and the $I(V)$ curve at RT after cooling down (blue curve) of two samples: 2T-8020 and 2T-9010. In the left plot, referring to 2T-8020, the blue curve has clearly a greater slope (conductance) on behalf of the red curve; conversely, the right plot referring to 2T-9010 displays perfectly superimposing curves for the two measurements. The discrepancy in the resistance measured for the

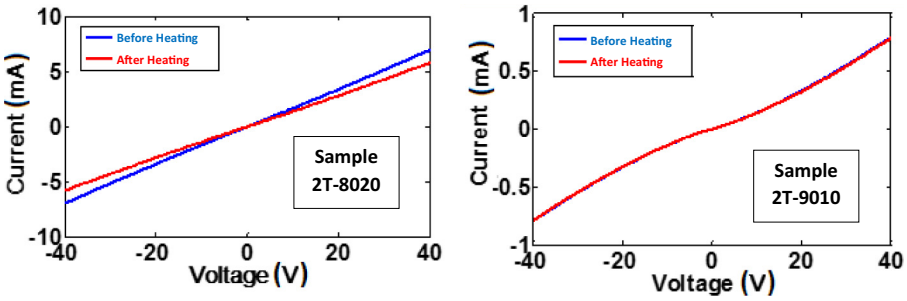

Fig. 3. On the left graph, I/V curves of the sample 2T-8020 taken at about room temperature during the first phase of increasing Heating Steps (red curve) and the second phase of decreasing Cooling Steps (blue curve). On the right graph, I/V curves of the sample 2T-9010 taken at the same conditions of the adjacent graph. (For interpretation of the references to color in this figure legend, the reader is referred to the web version of this article.)

2T-8020 film is almost 15% and is due to the increase of black diamond electrical conductivity properties happening intrinsically with the high temperature regime imposed during the measurements. We underline that the 2T-6633 behavior has not been shown in this section because, for sake of simplicity, it was directly proofed according to the temperature test discussed in the next paragraph, where we will show that it behaves similarly to 2T-8020 sample.

The aforesaid current increment, observed after the cooling down of 2T-BD samples with lower fraction of absorbed laser energy during the first treatment, thus excluding the completely stable 2T-9010, was mainly due to a significant decrease of E_{a2} (see Fig. 4). In particular, for the more insulating 2T-5050 sample the E_{a2} practically halves from 1.74 eV to 0.95 eV; same behavior for the 2T-8020 with E_{a2} that halves from 0.69 eV to 0.33 eV. The activation energies in the cooling phase are reported in Table 2. The diminution of the E_{a2} value induced a decrease of the resistance at room temperature estimated to be as large as 0.7 decades for the 2T-5050. We attribute this behavior to the major absorbed energy over the surface in the second texturing, that considering the rapid cooling during the LIPPS creation process, does not allow the diamond lattice atoms to stabilize in the best possible configuration. The presence of residual strain that needs to be released is demonstrated by the Raman analysis reported in Section 3.3. The sample with higher energy adsorbed in the second texturing will be the subject of a major change in the conductivity properties.

In order to give a reference value for order of magnitude of conductivity for the 2T-BD samples, we calculated that in order to match the best nitrogen-doped UNCD films ($\sigma = 200$ S/cm) we should consider an active thickness equal to 78 nm for the minimum measured resistance (2T-8020). On the other hand, the conductive layer is supposed to be almost 2D, collocating 2T-BD in the gap between UNCD (10^2 S/cm) and graphene (10^6 S/cm). However, since we do not know the real depth involved in the conduction, a real comparison has to be postponed.

3.2. Effect of thermal annealing

For the samples that demonstrated to have different behavior during the measurements in the heating and in the cooling phase, we added a conductivity test at the highest temperatures. In particular, the more unstable samples were the films that absorbed a higher amount of accumulated fluence: the 2T-5050, the 2T-8020 and the 2T-6633. Conversely, the 2T-9010 specimen demonstrated a good temperature electric conduction stability. Subjected to the high temperature test, these samples showed a continuous increase of conductivity during the thermal annealing. We monitored the current in the samples at the absolute voltage of 1 V keeping them at high temperature (about 500 °C) for more than one day. In order to avoid measurement artifacts due to charge accumulation on one of the electrodes, we avoided to maintain a fixed biasing, periodically alternating between ± 1 V. The conductance change behavior is very similar both for 2T-8020 and for 2T-6633 (shown in Fig. 5), with a percentage change in the first 8 h of 1.4% and 1.5% per hour, respectively (calculated considering mean variation $\Delta I/\Delta t$). Both values tend to decrease and the conductance percentage change slows down to 0.62% for the 2T-8020 and to 0.46% for the 2T-6633 in the last 8 h. In terms of current absolute change, we have 2.85 μA/h for the 2T-6633 and 5 μA/h for the 2T-8020.

A little different treatment has been reserved to the sample 2T-5050 where the total resistance of the sample was much higher than the samples 2T-8020 and 2T-6633. In this case we applied always both positive and negative voltages but with an absolute value of 10 V instead of 1 V. The values of current corresponding to the positive voltage measurements are shown in Fig. 5c. The percentage change of the 2T-5050 sample is much higher than the value found for previous samples and reaches an absolute value of 23% per hour. Since the current increment did not show any slowdown during the overall time of the annealing as in the previous cases, we elongated the test time to almost one week. It is possible to note that the current changed of two orders of magnitude from 40 nA to almost 4 μA. The final slope value is even higher than the initial one: the current increment rate passes from

Table 2
Activation energy of the BD samples as measured during the cooling phase.

Sample	*Low temperature range*		*High temperature range*	
	E_{a1} *(eV)*	G_{PreF1} *(S)*	E_{a2} *(eV)*	G_{PreF2} *(S)*
2T-8020	18 m	0.37 m	0.33	0.014
2T-5050	0.37	32 n	0.95	7.4 m

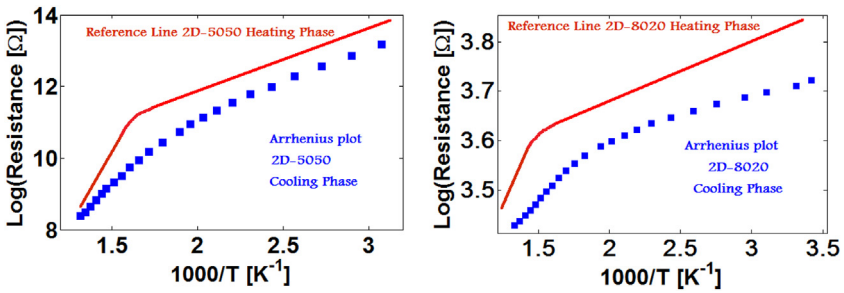

Fig. 4. Left graph shows the monitored resistance of the sample 2T-5050 during the cooling phase from 775 K to RT. Right graph shows the same for the sample 2T-8020.

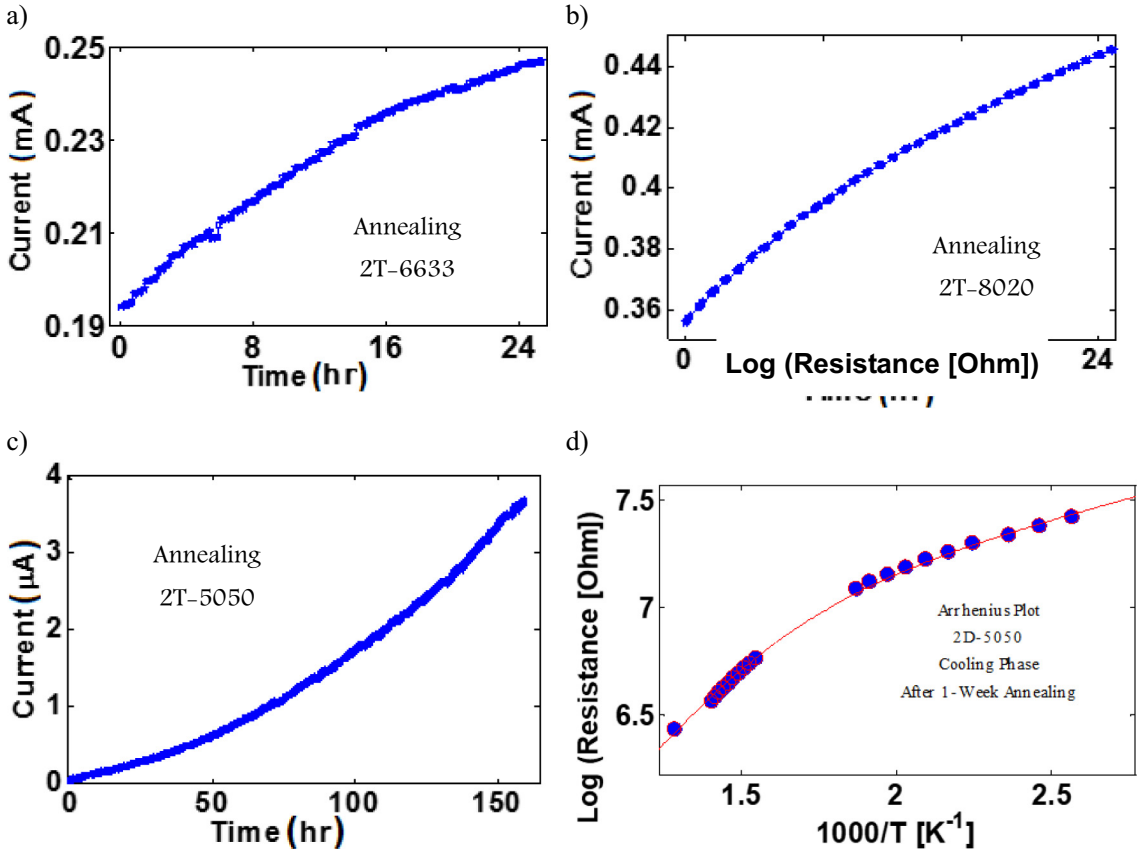

Fig. 5. Monitored annealing @ 775 K of the sample 2T-6633 (a); 2T-8020 (b); 2T-5050 (c). The applied voltage was ± 1 V for a) and b) and ± 10 V for c). d) shows the Arrhenius plot for the 2T-5050 sample during the cooling phase from 775 K to RT after the annealing.

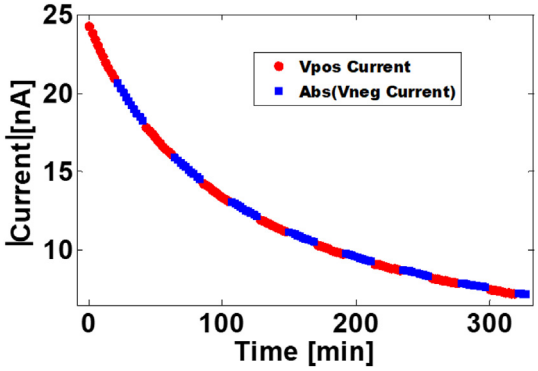

Fig. 6. 2T-5050 current behavior after cooling from 800 K to room temperature at the alternating biasing voltages of +10 V (red circles) and −10 V (blue squares). (For interpretation of the references to color in this figure legend, the reader is referred to the web version of this article.)

10 nA/h to 38 nA/h at the end of the week, even if the percentage change decreases from 23% to 1.2% per hour. Therefore, the behavior of 2T-5050 is different from the other samples both in the order of magnitude of conductance that in the conductance increment with time. If we consider the non-linear effect on conductivity related to the active hopping sites ordering, the release of thermal energy with annealing time may affect more or less the conductivity according to the present variance of the atomic bonding disposition in the lattice. In fact, if we analyze deeply the second derivative of the 2T-5050 current increment, it passes from positive values to negative ones close to the end of the 7 days of annealing, thus resembling the concave nature of Fig. 5a) and b). It is realistic to think that, if annealed for one month, arriving to a major happened readjustment of the lattice, its increment would slow down to the level of the other two BD samples. It is worth to stress that the main conductive mechanism of the other 2T-BD samples (that in the meV range) is not present in the initial state of 2T-5050 indicating that the bonding disposition of the carbon atoms in its surface is largely different from the other ones.

Because of the significant variation in total conductivity, we performed again Arrhenius measurements during the cooling phase of this sample (see Fig. 5d). That high current increment corresponded in a high variation of the two activation energies that passed from 0.37 eV to 76 meV and from 0.95 eV to 0.39 eV, almost retracing the activation energy values reported previously for the cooling phase of the 2T-8020 sample but with a conductance difference of about three orders of magnitude. The closeness in value between E_{a1} pre-annealing (0.39 eV) and E_{a2} post-annealing (0.37 eV) induces to think that the same physical phenomenon is at the base of the electric conductivity in the two temporally different measurements of the same sample. The change is in the temperature range where this activation energy prevails over the other mechanisms, that shifts to lower temperatures.

Because of a peculiar behavior in the last two points close to RT of the Arrhenius steps, sample 2T-5050 was monitored (still in vacuum) also at RT after the 1-week annealing. It surprisingly released great part of the conductivity increment (see Fig. 6). We recall this sample is the one that completely changed the disposition of the ripples from horizontal to vertical by the two successive laser treatments. We underline that the 2T-5050 was the only sample in which the conductance increment was partially lost in vacuum at RT, while the other samples if measured by multimeter in air were stable even after weeks.

Resuming, it seems that the samples have a common tendency in increasing the electric conductivity and reducing the activation energies under the action of a thermal energy given to the produced black

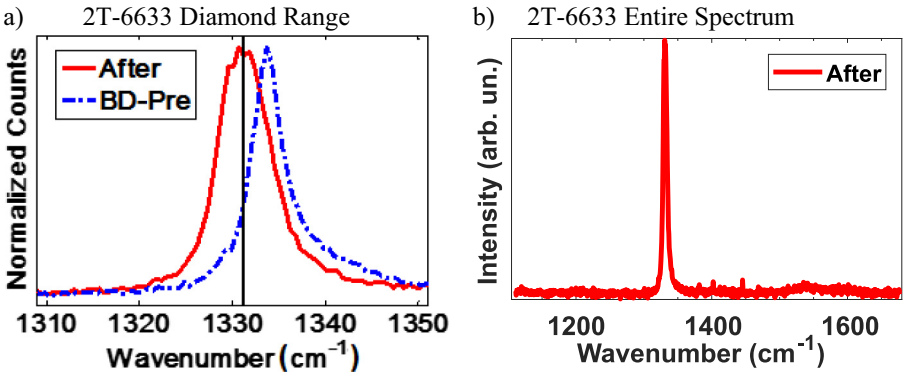

Fig. 7. a) Zoom of Raman spectra around diamond natural resonance for the 2T-6633 sample: as-fabricated (blue dash-dot line) and after thermal measurements (continuous red line). b) Complete Raman spectra after thermal measurements showing the absence of other significant contributions in the spectrum. (For interpretation of the references to color in this figure legend, the reader is referred to the web version of this article.)

diamonds after laser treatments. The final activation energy in the high temperature range is almost equal for all the samples and it falls in the 0.3–0.45 eV gap. This value is attributed to the presence of defects acting as electron traps.

3.3. Raman spectroscopy

In order to investigate lattice variations and possible relaxations induced by the thermal annealing, causing the studied modification of films' electric properties, we performed multiple Raman measurements on the samples in the gap between the two electrodes, by choosing five points from one side of the diamond square substrate to the other one. The overall compressive stress observed in as-fabricated black diamond samples [17], appears in Raman spectra as an asymmetry of the peak profile towards higher wavenumbers.

In Fig. 7a) we report the zoom of the Raman spectra, acquired from 1100 cm^{-1} to 1676 cm^{-1}, around the diamond reference peak of 1331.2 cm^{-1}. The analyzed spot collocates in the central point of the gap between the silver rectangular contacts. It is worth to observe that Raman spectra acquired for the samples after the thermal measurements described above, reported as red curves in Fig. 7, have a well-defined symmetrical behavior around the reference line indicating the absence of residual strain. There is a clear overall shift of the Raman signal towards lower wavenumbers and the disappearance of the splitting of the diamond peak into compressive and tensile peaks [18].

It must be underlined that, although the Raman analysis makes evident that a readjustment of the lattice occurred for all the samples after the thermal annealing, it does not completely explain why the difference in electronic properties between all the samples. In fact, 2T-9010 sample shows a lower but similar Raman variation of 2T-6633, but the first one showed conductance practically stable in temperature, while the second one showed thermally tunable conductivity. Therefore, we cannot really explain conductivity changes as increases of charge mobility due to lattice stresses relaxation. A comparison between the compressive stresses in the various samples was performed by fitting with multiple Gaussian profiles the Raman peak present around 1332 cm^{-1} and calculating the percentage of the stress signal before and after the thermal treatment and it is reported in Table 3.

In Table 3 it is evident the difference in the stability of lattice strains between the various samples. In fact, the samples created with a minor absorption of the laser fluence in the fabrication process (2T-9010 and 2T-8020) were able to recover completely and almost completely from induced strain, while the other two samples keep a good percentage of strained covalent bonds.

We extended the Raman measurement to wavenumbers up to 1700 cm^{-1} in order to evaluate the possible presence of graphite formation (see Fig. 7b). We found only one of the twenty measured points with a clear graphite band and in the sample with the lower conductance (i.e. 2T-5050). Formation of graphite on the surface during the thermal treatment, as a main actor of the conductivity transformation, has to be excluded.

Table 3
Contribution of the fitted Gaussians of the BD samples as measured in Raman spectra.

Sample	*Before thermal treatment*		*After thermal treatment*	
	1331–2 cm^{-1}	*Stress*	*1331–2 cm^{-1}*	*Stress*
2T-9010	58.8%	41.2%	100%	0%
2T-8020	12.8%	87.2%	94.1%	5.9%
2T-6633	0%	100%	66.4%	32.6%
2T-5050	53.9%	46.1%	67.5%	32.5%

4. Conclusions

We performed electrical conductivity measurements in the temperature range from 300 to about 800 K for 2T-BD samples obtained by thermal-grade diamond films, on which LIPSS along two perpendicular directions with different modality of released laser-energy was produced on the surface. Such analysis highlighted a similar behavior for almost all the samples with a low activation energy (of the order of tens meV) in the low temperature regime (300–500 K), in many cases comparable to the RT thermal energy and thus attributing at RT a considerable surface conductivity to the BD films.

A second activation energy ranging from 0.45 eV to 0.75 eV was found at the highest temperature range (550–800 K), which halves rapidly along with the thermal treatment in the samples with higher absorbed laser energy and further reduces after prolonged annealing. Compared to the others, 2T-5050 sample depicted a different behavior, showing an initially much lower conductance and higher activation energy values. Conversely, it highlighted the highest thermal activation rate, and, after thermal treatment, its resistance thermal trend was characterized by activation energies comparable to those found in the other samples, with E_{a1} in the meV range and E_{a2} in the 0.3–0.4 eV gap.

Finally, the low values found for E_{a1} let us induce to hypothesize a charge hopping from defect to defect as the main mechanism transport in 2T-BD. Such an assumption can be tentatively confirmed by the absence of a DC Hall effect in 2T-BD samples at RT, in agreement with many studies about hopping conduction transport [19]. This has to be still demonstrated by extending the measurements down to cryogenic temperatures to be performed in the near future. These results would pave the way to the possibility of thermal processing of black diamond plates to tune electronic transport properties both for high temperature and for RT utilization.

Acknowledgements

The activity was supported by the European Union FP7 FET-Energy Project ProME3ThE2US2 "*Production Method of Electrical Energy by Enhanced Thermal Electron Emission by the Use of Superior*

Semiconductors", Grant Agreement n. 308975.

References

[1] D. Trucchi, A. Bellucci, M. Girolami, M. Mastellone, S. Orlando, Surface texturing of CVD diamond assisted by ultrashort laser pulses, Coatings 7 (2017) 185, https://doi.org/10.3390/coatings7110185.

[2] J.W. Schwede, I. Bargatin, D.C. Riley, B.E. Hardin, S.J. Rosenthal, Y. Sun, F. Schmitt, P. Pianetta, R.T. Howe, Z.X. Shen, N.A. Melosh, Photon-enhanced thermionic emission for solar concentrator systems, Nat. Mater. 9 (2010) 762–767, https://doi.org/10.1038/nmat2814.

[3] G. Segev, Y. Rosenwaks, A. Kribus, Limit of efficiency for photon-enhanced thermionic emission vs. photovoltaic and thermal conversion, Sol. Energy Mater. Sol. Cells 140 (2015) 464–476, https://doi.org/10.1016/J.SOLMAT.2015.05.001.

[4] P. Calvani, A. Bellucci, M. Girolami, S. Orlando, V. Valentini, R. Polini, D.M. Trucchi, Black diamond for solar energy conversion, Carbon 105 (2016) 401–407, https://doi.org/10.1016/j.carbon.2016.04.017.

[5] P. Calvani, A. Bellucci, M. Girolami, S. Orlando, V. Valentini, R. Polini, D.M. Trucchi, Absorptance enhancement in fs-laser-treated CVD diamond, Phys. Status Solidi Appl. Mater. Sci. 212 (2015) 2463–2467, https://doi.org/10.1002/pssa.201532189.

[6] J.A. Vonwindheim, V. Venkatesan, D.M. Malta, K. Das, Electrical characterization of semiconducting diamond thin-films and single-crystals, J. Electron. Mater. 22 (1993) 391–398.

[7] E.P. Visser, G.J. Bauhuis, G. Janssen, W. Vollenberg, J.P. van Enckevort, L.J. Giling, Electrical conduction in homoepitaxial, boron-doped diamond films, J. Phys. Condens. Matter 4 (1992) 7365 http://stacks.iop.org/0953-8984/4/i=36/a=011.

[8] J.-P. Lagrange, A. Deneuville, E. Gheeraert, Activation Energy in Low Compensated Homoepitaxial Boron-doped Diamond {films1Paper} Presented at the Diamond 1997 Conference.1, 7 (1998), pp. 1390–1393, https://doi.org/10.1016/s0925-9635(98)00225-8.

[9] T.H. Borst, O. Weis, Electrical characterization of homoepitaxial diamond films doped with B, P, Li and Na during crystal growth, Diam. Relat. Mater. 4 (1995) 948–953, https://doi.org/10.1016/0925-9635(94)00263-0.

[10] K. Thonke, The boron acceptor in diamond, Semicond. Sci. Technol. 18 (2003), https://doi.org/10.1088/0268-1242/18/3/303.

[11] P.K. Sitch, G. Jungnickel, M. Kaukonen, D. Porezag, T. Frauenheim, M.R. Pederson, K.A. Jackson, A study of substitutional nitrogen impurities in chemical vapor deposited diamond, J. Appl. Phys. 83 (1998) 4642–4646, https://doi.org/10.1063/1.367249.

[12] S. Bhattacharyya, O. Auciello, J. Birrell, J.A. Carlisle, L.A. Curtiss, A.N. Goyette, D.M. Gruen, A.R. Krauss, J. Schlueter, A. Sumant, P. Zapol, Synthesis and characterization of highly-conducting nitrogen-doped ultrananocrystalline diamond films, Appl. Phys. Lett. 79 (2001) 1441–1443, https://doi.org/10.1063/1.1400761.

[13] M. Mertens, M. Mohr, N. Wiora, K. Brühne, H.J. Fecht, N-type conductive ultrananocrystalline diamond films grown by hot filament CVD, J. Nanomater. 2015 (2015), https://doi.org/10.1155/2015/527025.

[14] T. Ikeda, K. Teii, C. Casiraghi, J. Robertson, A.C. Ferrari, Effect of the sp2 carbon phase on n-type conduction in nanodiamond films, J. Appl. Phys. 104 (2008) 1–7, https://doi.org/10.1063/1.2990061.

[15] M. Girolami, A. Bellucci, M. Mastellone, S. Orlando, V. Valentini, R.M. Montereali, M.A. Vincenti, R. Polini, D.M. Trucchi, Optical characterization of double-nano-textured black diamond films, Carbon (2018), https://doi.org/10.1016/j.carbon.2018.07.055.

[16] D.M. Trucchi, A. Bellucci, M. Girolami, P. Calvani, E. Cappelli, S. Orlando, R. Polini, L. Silvestroni, D. Sciti, A. Kribus, Solar thermionic-thermoelectric generator (ST2G): concept, materials engineering, and prototype demonstration, Adv. Energy Mater. 8 (2018) 1–14, https://doi.org/10.1002/aenm.201802310.

[17] M. Girolami, A. Bellucci, M. Mastellone, S. Orlando, V. Valentini, R.M. Montereali, M.A. Vincenti, R. Polini, D.M. Trucchi, Impact of laser wavelength on the optical and electronic properties of black diamond, Phys. Status Solidi Appl. Mater. Sci. 214 (2017) 1–7, https://doi.org/10.1002/pssa.201700250.

[18] A. Bellucci, P. Calvani, M. Girolami, S. Orlando, R. Polini, D.M. Trucchi, Optimization of black diamond films for solar energy conversion, Appl. Surf. Sci. 380 (2016) 8–11, https://doi.org/10.1016/j.apsusc.2016.02.107.

[19] H. Fritzsche, N.F. Mott, E.A. Davis (Eds.), Electronic Processes in Non-crystalline Materials, xiv Oxford University Press, New York, 1971, , https://doi.org/10.1126/science.176.4039.1117 438 pp., illus. $24. International Series of Monographs on Physics, Science (80-.). 176 (1972) 1117.